

## Evaluation of moisture in the Hadley Centre climate model using simulations of HIRS water-vapour channel radiances

By RICHARD P. ALLAN<sup>1</sup>\*, M. A. RINGER<sup>1</sup> and A. SLINGO<sup>2</sup>

<sup>1</sup>Hadley Centre, Met Office, Exeter, UK

<sup>2</sup>ESSC, University of Reading, UK

(Received 20 November 2002; revised 7 April 2003)

### SUMMARY

It is important to establish that climate models can accurately simulate the observed present-day fluctuations of water vapour. In particular, water-vapour and cloud-radiative feedbacks are intrinsically linked to processes governing relative-humidity distribution and variability. To explore these issues, clear-sky radiances, sensitive to upper-tropospheric relative humidity, are simulated within the Hadley Centre atmospheric climate model, version HadAM3, allowing direct comparison with High Resolution Infrared Sounder (HIRS) observations. The model is forced by observed sea surface temperatures and sea-ice fields over the period 1979–98. Evaluation of the simulated distribution and variability of water vapour is undertaken utilizing the HIRS 6.7  $\mu\text{m}$  brightness temperature ( $T_{6.7}$ ) and satellite measurements of column-integrated water vapour and clear-sky outgoing long-wave radiation (OLR). Modifications are made to the clear-sky OLR and  $T_{6.7}$  HadAM3 diagnostics to reduce sampling inconsistencies with the observed products. Simulated  $T_{6.7}$  over subtropical dry zones are higher than  $T_{6.7}$  from observations, particularly in the southern hemisphere, and is symptomatic of an overactive circulation. The observed spatial signature of the  $T_{6.7}$  interannual variability is dominated by El Niño and is captured well by HadAM3. Interannual variability of the tropical ocean mean  $T_{6.7}$  is consistent between HadAM3 and the HIRS observations, suggesting that the small simulated decadal changes in relative humidity are realistic.

KEYWORDS: Clear-sky sampling Long-wave radiation Relative humidity

### 1. INTRODUCTION

Upper-tropospheric relative humidity (UTH) plays a fundamental role in determining both water-vapour and cloud feedbacks, which have the potential to either amplify or reduce the climate sensitivity to a radiative forcing (e.g. IPCC 2001). An important stage in improving our confidence in these feedback processes is to evaluate model simulations of the present-day climate. Climate models can generally represent the observed response of column-integrated water vapour (CWV) to ocean surface temperature (e.g. Soden 2000a; Wentz and Schabel 2000). This is not surprising because of the strong coupling between the ocean surface and the lower troposphere (which contains the majority of atmospheric moisture) and the robust physical relationship between saturated water-vapour pressure and temperature described by the Clausius–Clapeyron equation. However, radiative cooling to space is sensitive to moisture changes throughout the troposphere (e.g. Shine and Sinha 1991; Allan *et al.* 1999) and changes in UTH are important in determining cloud distribution and variability (e.g. Udelhofen and Hartmann 1995), which further perturb the top-of-atmosphere radiation budget. For further discussion of water-vapour feedback see Held and Soden (2000).

In the free troposphere, coupling with the surface is not well understood; direct observations of UTH by radiosonde are generally of low accuracy, owing to the poor instrument response at low temperature and moisture values (Spencer and Braswell 1997), and the measurement of long-term changes is impeded by data distribution and continuity issues (Elliot 1995; Bauer *et al.* 2002). Nevertheless, some studies have used these data to suggest an inadequacy of climate model simulations of UTH and in the coupling of moisture and temperature in the upper troposphere with the surface (e.g. Sun and Held 1996), although such analyses do not properly take observed sampling into

\* Corresponding author, present affiliation: Environmental Systems Science Centre, Harry Pitt Building, 3 Earley Gate, Whiteknights, Reading, Berkshire RG6 6AL, UK. e-mail: rpa@mail.nerc-essc.ac.uk  
© Crown copyright, 2003.

account. While other studies have suggested that the water-vapour feedback in climate models is robust (e.g. Ingram 2002; Soden *et al.* 2002), it is still not clear that different climate models produce consistent height-dependent temperature and water-vapour responses to present-day temperature variability (Allan *et al.* 2002).

Satellite radiances potentially provide an independent means of testing the water-vapour simulation by models. The 6.7  $\mu\text{m}$  region of the long-wave spectrum exhibits strong sensitivity to UTH, particularly over low latitudes. Soden and Bretherton (1993) derived the following relationship to estimate UTH from the 6.7  $\mu\text{m}$  brightness temperature ( $T_{6.7}$ ) given by geostationary satellite:

$$\text{UTH} = \frac{\beta}{P_0} \cos \theta \exp(a + bT_{6.7}), \quad (1)$$

where  $\theta$  is the satellite viewing angle,  $a$  and  $b$  are constants and the  $\beta/P_0$  terms account for the dependence of  $T_{6.7}$  on atmospheric temperature (see Jackson and Bates (2001) for discussion). Adjusting radiance measurements to equivalent nadir view ( $\cos \theta = 1$ ) and incorporating  $\beta$  into the regression coefficients  $a$  and  $b$ , Soden and Fu (1995) highlighted a strong link between UTH, deep convection and the greenhouse effect by combining data from the TIROS\* Operational Vertical Sounder High-resolution Infrared Sounder (HIRS) 6.7  $\mu\text{m}$  channel with other satellite products. Bates and Jackson (1997) developed the HIRS-derived UTH data for 1979–94, along with satellite column water-vapour data to evaluate the performance of a number of atmospheric climate models forced by observed sea surface temperatures. More recently, Bates *et al.* (2001) extended the HIRS 6.7  $\mu\text{m}$  UTH record from 1979–98, accounting for the temperature dependence of  $T_{6.7}$  by using HIRS channel-6 (15  $\mu\text{m}$ ) brightness temperature. Using this method, attempts were made to diagnose trends from the HIRS UTH data (Bates and Jackson 2001).

In the present study we use the 20-year HIRS  $T_{6.7}$  record along with additional satellite data to extend previous evaluations of moisture simulated by the Hadley Centre climate model (e.g. Bates and Jackson 1997; Pope *et al.* 2001). An important advance over such studies is the explicit simulation of the HIRS 6.7  $\mu\text{m}$  (channel-12) radiances within the model, thus avoiding errors introduced in the derivation of UTH and subsequent comparison with model humidity. Previous simulations of  $T_{6.7}$  were computed off-line using monthly mean (e.g. Chen *et al.* 1996) or daily mean (e.g. Salathé *et al.* 1995) climate model output and were subject to a number of sampling limitations (e.g. Engelen *et al.* 2000). In the present study we use a more sophisticated radiation code applied at a higher spatial and temporal resolution. Additionally, we account for the most important sampling differences between model and satellite data, enabling us to assess more accurately the realism of moisture distribution and variability in the Hadley Centre climate model. A comparable evaluation of moisture in the National Center for Atmospheric Research (NCAR) Community Climate Model has also recently been conducted over a much shorter period than the present study (Iacono *et al.* 2003).

## 2. CLIMATE MODEL AND OBSERVATIONAL DATA

### (a) *Experimental design*

We employed the Hadley Centre atmospheric climate model, version HadAM3 (Pope *et al.* 2000), at the standard resolution of 2.5° latitude by 3.75° longitude in

\* Television Infrared Observation Satellite.

the horizontal and 19 levels in the vertical. The model was forced using observed sea surface temperature (SST) and sea-ice distributions for 1978–99 from HadISST\* (Rayner *et al.* 2003). Climatological aerosols, a seasonally varying climatology of zonal-mean ozone profiles (Li and Shine 1995) and 1990 concentrations of greenhouse gases were prescribed. A three-member ensemble was created using different initial input for each run. An additional experiment containing realistic changes in greenhouse gases, tropospheric and stratospheric ozone, direct and indirect sulphate aerosols, solar irradiance and volcanic aerosols over the period 1978–99 was also included in some of the analysis. Details of the experimental design are contained in Allan and Slingo (2002).

In all HadAM3 experiments, an enhanced version of the Edwards and Slingo (1996) radiation code was used within HadAM3 to simulate HIRS channel-12 nadir clear-sky radiances at every radiation time step (3 h). The technique was described by Ringer *et al.* (2002). Off-line tests of the radiance code produced differences from line-by-line calculations of 0.13 K for a standard tropical profile and 0.15 K and 0.07 K for midlatitude summer and winter standard atmospheric profiles. The output radiances were converted to 6.7  $\mu\text{m}$  brightness temperatures at every radiation time step for consistency with the HIRS  $T_{6,7}$  dataset from Bates *et al.* (2001).

#### (b) *Satellite and reanalysis data*

We used the 1979–98 HIRS Pathfinder version 1 intercalibrated  $T_{6,7}$  data from Bates *et al.* (2001); 500 hPa vertical velocity  $\omega_{500}$  for the same period was taken from the National Centers for Environmental Prediction (NCEP) NCAR 40-year reanalysis (Kalnay *et al.* 1996). Clear-sky outgoing long-wave radiation (OLR) from the Earth Radiation Budget Satellite (ERBS) (Barkstrom *et al.* 1989) for the period 1985–89, the Scanner for Radiation Budget (ScaRaB) (Kandel *et al.* 1998) for 1994–95 and the Clouds and the Earth's Radiant Energy System (CERES) (Wielicki *et al.* 1996) for 1998 were also used. Column-integrated water vapour from the Scanning Multichannel Microwave Radiometer (SMMR) (Wentz and Francis 1992) for 1979–84 and the Special Sensor Microwave Imager (SSM/I) (Wentz 1997) for 1987–98 were included in the comparisons.

#### (c) *Sampling issues*

Sampling inconsistencies between satellite measurements and model simulations potentially reduce the reliability of comparisons between these data. We performed preliminary integrations of HadAM3 to quantify some of the sampling differences and attempt to minimize these differences by applying modifications to standard model diagnostics.

(i) *Temporal sampling.* The HIRS instruments were flown aboard polar-orbiting platforms which, depending on there being one or two satellites in operation, provide 2–4 samples per day nominally at fixed local times. Attempt was made by Bates *et al.* (2001) to correct for drifts in the satellite orbits which cause the satellite overpass times to change with time. Regardless of these corrections, given that UTH shows diurnal changes relating to convective activity (e.g. Soden 2000b), inadequate sampling of  $T_{6,7}$  may cause biases in the monthly mean product. Using three-hourly model output for January 1998 we constructed monthly mean values of  $T_{6,7}$  using only data from within one hour of the actual satellite overpass times and compared these with the standard

\* Hadley Centre global sea-Ice and Sea Surface Temperature dataset.

monthly mean values. Although not an exact mapping of the satellite tracks, this method does provide a useful estimate of the potential sampling biases. Consistent with previous studies (e.g. Engelen *et al.* 2000) we find that differences between the two methods are small: for a two-satellite combination the differences are 0.03 K (less than 1% of the global (r.m.s.) model-minus-observation difference). This increases for a single satellite but still remains below about 0.15 K (5% of the model minus observation global r.m.s. difference). It should be noted that the impact of temporal sampling biases depends on the satellite channel being considered (Engelen *et al.* 2000). However, based on our analysis, we decided against the accurate simulation of HIRS  $T_{6,7}$  temporal sampling. Doing so may in fact introduce additional bias due to inaccuracies in the model diurnal cycle of convection and UTH (Yang and Slingo 2001).

(ii) *Clear-sky sampling bias.* Model clear-sky diagnostics are calculated at each radiation time step by setting cloud fraction to zero in the radiation scheme. However, satellite measurements of clear-sky OLR and  $T_{6,7}$  are not possible where cloud cover is extensive. Since cloudiness is correlated with relative humidity, the lack of measurements from these humid, low-emission points will introduce a positive bias into clear-sky OLR and  $T_{6,7}$  observational data. In a modelling study, Cess and Potter (1987) estimated the clear-sky OLR sampling bias was of order 1–2 W m<sup>-2</sup> in the global mean. The sampling bias can be as large as 10–15 W m<sup>-2</sup> for some dynamical regimes such as tropical convection (Allan and Ringer 2003). Utilizing radiosonde measurements, Lanzante and Gahrs (2000) estimated the magnitude of this effect to be 5–10% UTH in the most convective regions of the Tropics (or about 1 K  $T_{6,7}$  bias).

Here we assess this clear-sky bias effect on clear-sky OLR and  $T_{6,7}$  by utilizing the three-hourly HadAM3 output for January 1998. We cannot fully simulate the satellite clear-sky sampling since the satellite pixels are far smaller than the model grid points, so we instead estimate the magnitude of an important component of the clear-sky bias. We use two methods to approximate the satellite clear-sky sampling. In the first technique we retain three-hourly values only if cloud fraction is below a critical threshold  $C$ . Subsequently the remaining clear-sky data are averaged at each grid point. We construct separate monthly means for each of the eight radiation time steps during the day from which we form a total monthly mean value. This avoids preferentially sampling particular local times during the day, although we find that applying a simple mean gives similar results. This technique is similar to that described in Iacono *et al.* (2003) who use  $C = 0.3$  but only consider clouds at altitudes higher than 750 hPa. In the second technique we weight the three-hourly data at each grid point by clear-sky fraction. Therefore a totally clear time step will receive maximum weighting and an overcast time step will receive zero weighting at each grid point. The zonal-mean differences relative to the standard clear-sky diagnostics are shown in Fig. 1 for the clear-sky fraction weighting technique and the threshold method for  $C = 0.05$  and  $C = 0.5$ .

The monthly mean clear-sky OLR and  $T_{6,7}$  sampling bias show similar latitudinal structure with a 2 W m<sup>-2</sup> clear-sky OLR bias being roughly equivalent to a 1 K bias in brightness temperature. The bias is generally positive over low latitudes because clear-sky times tend to correspond with lower humidity and therefore higher emission. However, for clear-sky OLR polewards of 50°N, the bias is negative. This is due mainly to land points which tend to be coldest under clear conditions in winter and therefore produce low emission. The clear-sky bias for  $C = 0.05$  is approximately double that of the  $C = 0.5$  case. Using the clear-sky weighting method, the calculated clear-sky bias is similar to the threshold method for  $C = 0.5$ . The  $T_{6,7}$  bias is approximately 1 K which is consistent with the 5–10% bias in UTH calculated by Lanzante and Gahrs (2000).

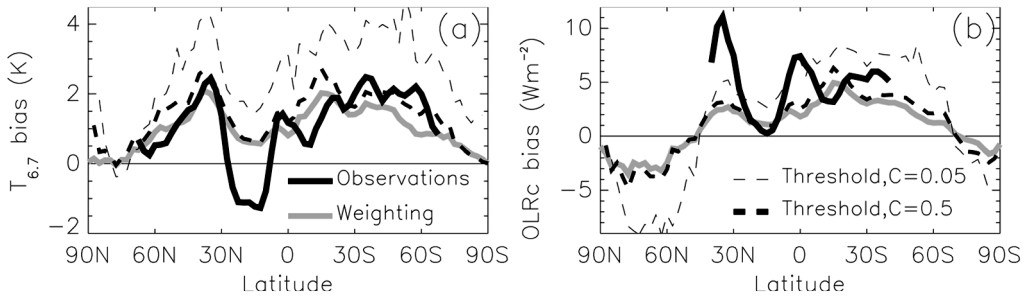


Figure 1. Zonal-mean clear-sky sampling bias for (a)  $T_{6,7}$  and (b) clear-sky outgoing long-wave radiation using weighting and threshold techniques for January 1998 (see text). The thin dashed lines only consider grid points of cloud fraction less than 5% while thick dashed lines use all grid points where cloud fraction is less than 50%. Thick grey lines show the bias when clear-sky quantities are weighted by the clear-sky fraction within a grid box. Thick black lines show (a) HIRS and (b) CERES observation minus model differences.

The HIRS clear-sky product used data only where cloud fraction was less than 75%. Thus, the  $C = 0.5$  tests may be more meaningful than the  $C = 0.05$  sub-sampling.

Also shown in Fig. 1 are the observed minus model differences for January 1998. The HIRS – HadAM3 differences for January 1998 appear to display a positive bias close to the  $C = 0.5$  case at many latitudes. The CERES minus HadAM3 clear-sky OLR differences are mainly within the  $C = 0.5$  and  $C = 0.05$  experimental range. Note that these tests do not account for moisture variation within the grid box, which is likely to increase the clear-sky bias, and cloud contamination of the radiances, which will to some extent compensate the clear-sky sampling bias. Also the observation-minus-model differences will include physical biases relating to atmospheric composition and circulation errors.

Whilst comparing all-sky OLR between models and observations avoids the clear-sky sampling inconsistencies, inaccurate simulation of cloud properties within HadAM3 will impede the meaningful evaluation of water vapour. Also, the robust nature of decadal variability in tropical OLR has yet to be established for observations and models (Wielicki *et al.* 2002). Therefore, based on the results presented in Fig. 1, it was decided to produce modified clear-sky OLR and  $T_{6,7}$  diagnostics using the clear-sky fraction weighting technique in addition to the standard diagnostics. The modified diagnostics are equivalent but not identical to the Type I method described in Cess and Potter (1987), while the standard diagnostics are referred to as Type II.

### 3. CLIMATOLOGY

Table 1 shows the 60°S–60°N area-weighted mean values and differences compared with the observations for each season over the entire domain and ocean only grid points. For clear-sky OLR and  $T_{6,7}$ , values are shown for Type I diagnostics but model-minus-observation differences are also shown for the standard Type II diagnostics (values in parentheses). Recall that the Type I diagnostic is more consistent with satellite clear-sky sampling than Type II. The model displays a negative  $T_{6,7}$  bias  $\leq 0.6$  K and r.m.s. difference below 2 K ( $< 1\%$  of the area-weighted mean) which is comparable with the 1982–84 analysis of the NCAR model by Iacono *et al.* (2003). The mean biases for Type II diagnostics are more than double those for Type I, while the r.m.s. Type II biases are approximately 50% greater than for the Type I differences. This illustrates the importance of the clear-sky sampling on the systematic model-minus-observation differences and adds confidence to the use of the modified Type I diagnostics. The annual

TABLE 1. AREA-WEIGHTED 60°S–60°N MEAN 6.7  $\mu\text{m}$  BRIGHTNESS TEMPERATURE  $T_{6.7}$  (K) (1979–98), CLEAR-SKY OUTGOING LONG-WAVE RADIATION  $\text{OLR}_c$  ( $\text{W m}^{-2}$ ) (1985–89), AND COLUMN-INTEGRATED WATER VAPOUR CWV ( $\text{kg m}^{-2}$ ) (1979–84 AND 1988–98), SIMULATED BY HADAM3 AND HADAM3-MINUS-OBSERVATION DIFFERENCES

Variable	Season	All Points			Ocean		
		HadAM3	Mean bias	r.m.s. bias	HadAM3	Mean bias	r.m.s. bias
$T_{6.7}$	DJF	245.9	−0.3 (−1.5)	1.8 (2.6)	246.5	−0.4 (−1.7)	1.7 (2.6)
	MAM	245.8	−0.4 (−1.7)	1.4 (2.3)	246.1	−0.4 (−1.7)	1.4 (2.4)
	JJA	246.4	−0.6 (−1.6)	1.9 (2.7)	246.2	−0.5 (−1.7)	1.7 (2.7)
	SON	246.2	−0.2 (−1.5)	1.6 (2.5)	246.5	−0.2 (−1.5)	1.7 (2.6)
$\text{OLR}_c$	DJF	268.0	−3.6 (−5.8)	6.8 (8.7)	273.1	−3.9 (−6.4)	5.2 (7.8)
	MAM	271.4	−3.5 (−6.1)	6.3 (8.3)	272.4	−3.2 (−5.9)	4.5 (7.1)
	JJA	274.4	−2.9 (−5.1)	5.7 (7.5)	271.6	−3.7 (−5.9)	5.0 (7.2)
	SON	271.9	−3.4 (−5.8)	6.1 (8.1)	272.6	−3.0 (−5.6)	4.5 (7.1)
CWV	DJF	26.0	–	–	28.8	0.1	2.6
	MAM	27.3	–	–	29.2	0.0	2.4
	JJA	28.9	–	–	29.4	0.5	2.4
	SON	26.9	–	–	28.4	0.1	2.5

The observations are interpolated to the model grid and differences calculated only at grid points which contain no missing data. From these differences, the mean bias and r.m.s. bias are calculated for the entire domain and ocean-only points. For clear-sky OLR and  $T_{6.7}$ , differences are shown for Type I and Type II diagnostics. Type II are within parentheses.

mean Type I bias for 40°S–40°N (not shown) is below 0.4 K, much smaller than the 2.2 K bias calculated by Salathé *et al.* (1995). Further, their difference is the opposite sign to that expected from the clear-sky sampling bias, suggesting unrealistic model profiles or inaccurate radiative computations.

The model-minus-satellite data clear-sky OLR difference is approximately 1% of the mean and the r.m.s. differences approximately 2% of the mean. The mean biases for Type II clear-sky diagnostics (values in parentheses) are significantly larger than those for the Type I diagnostics. CWV observations, available only over the oceans, do not show such a systematic bias in the area-weighted mean. This is possibly because the microwave instruments are able to provide accurate retrievals over cloudy regions and therefore provide a more consistent comparison with the model simulations, although they cannot accurately take measurements where precipitation is occurring. The systematic retrieval error for the SSM/I CWV data is estimated to be 0.6  $\text{kg m}^{-2}$  (Wentz 1997).

The climatologies of  $T_{6.7}$ ,  $\omega_{500}$ , clear-sky OLR and CWV for the climate model (mean of three-member ensemble) and the observations are shown for June–August (JJA) (Fig. 2) and December–February (DJF) (Fig. 3) seasons. Model-minus-observation differences are displayed in Fig. 4. First we compare  $T_{6.7}$  for the HIRS data and the HadAM3 simulations. Values are lowest at high latitudes where atmospheric temperatures are low and also over moist, tropical regions where emission originates from high altitudes where temperatures are also low. In the dry, subtropical regions,  $T_{6.7}$  greater than 250 K (shaded region) are widespread. This is due to weaker water-vapour absorption allowing greater emission from lower down in the tropical atmosphere where temperatures are high. Comparing Figs. 2 and 3, the  $T_{6.7} > 250$  K regions are found to be more widespread in the winter hemisphere in both observations and simulations. This is explained by a stronger Hadley circulation over the winter hemisphere (e.g. Chen *et al.* 1996).

There is a strong correspondence between  $T_{6.7}$  (panels (a) and (b) in Figs. 2 and 3) and the vertical motion  $\omega_{500}$  (panels (c) and (d)), which illustrates the strong dynamical

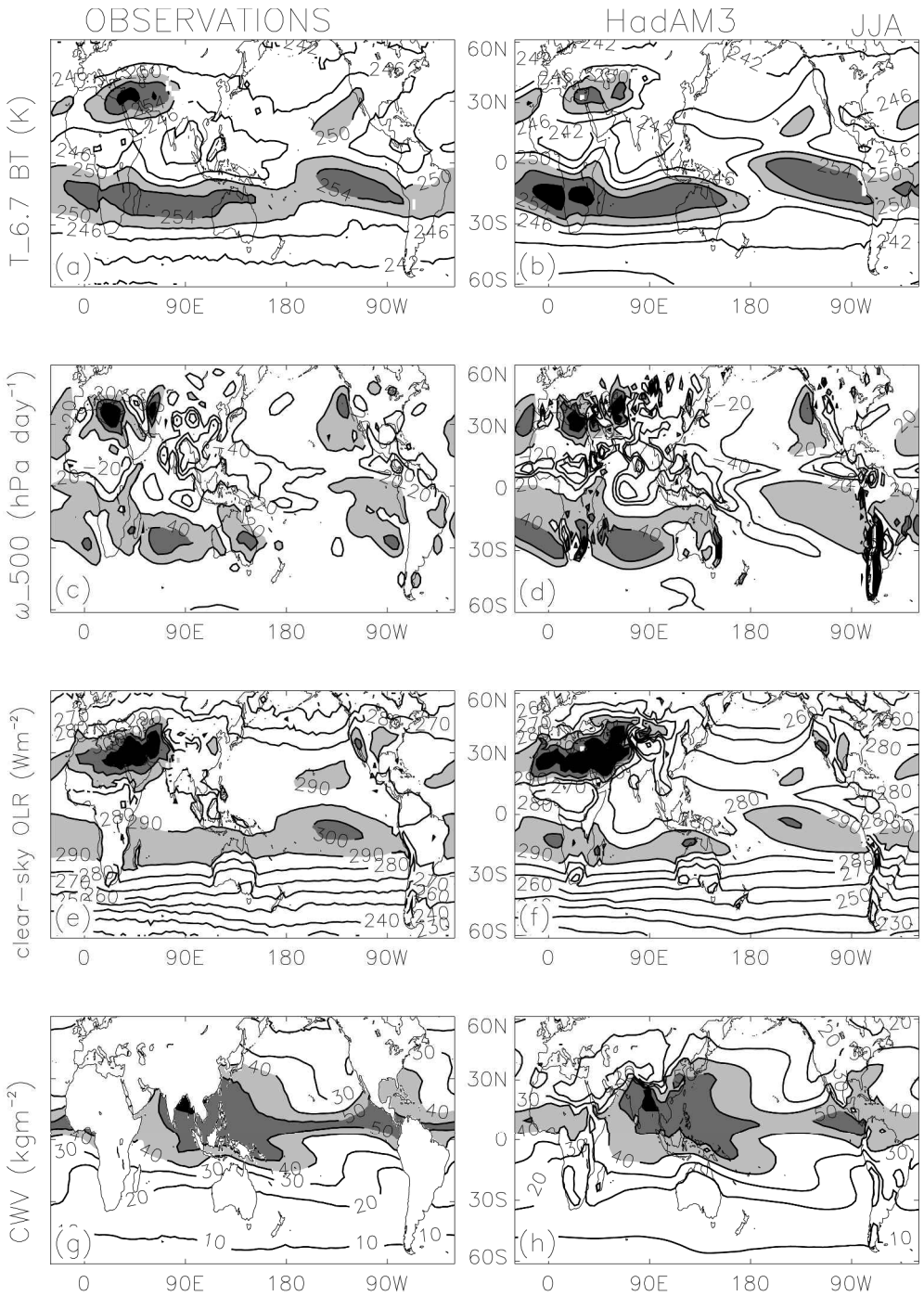


Figure 2. 1979–98 climatological fields for June–August:  $T_{6.7}$  (K) from (a) HIRS channel 12 and (b) simulated by HadAM3; 500 hPa vertical velocity (hPa d $^{-1}$ ) from (c) NCEP and (d) HadAM3. 1985–89 climatological fields of clear-sky outgoing long-wave radiation ( $\text{W m}^{-2}$ ) from (e) ERBS and (f) HadAM3. Climatological fields of CWV ( $\text{kg m}^{-2}$ ) covering the periods 1979–84 and 1988–98 from (g) the combination of SMMR and SSM/I and (h) from HadAM3. Shading denotes  $T_{6.7} > 250$  K,  $\omega_{500} > 20$  hPa d $^{-1}$ , OLR  $> 290$   $\text{W m}^{-2}$  and CWV  $> 40$   $\text{kg m}^{-2}$ . See text for explanation.

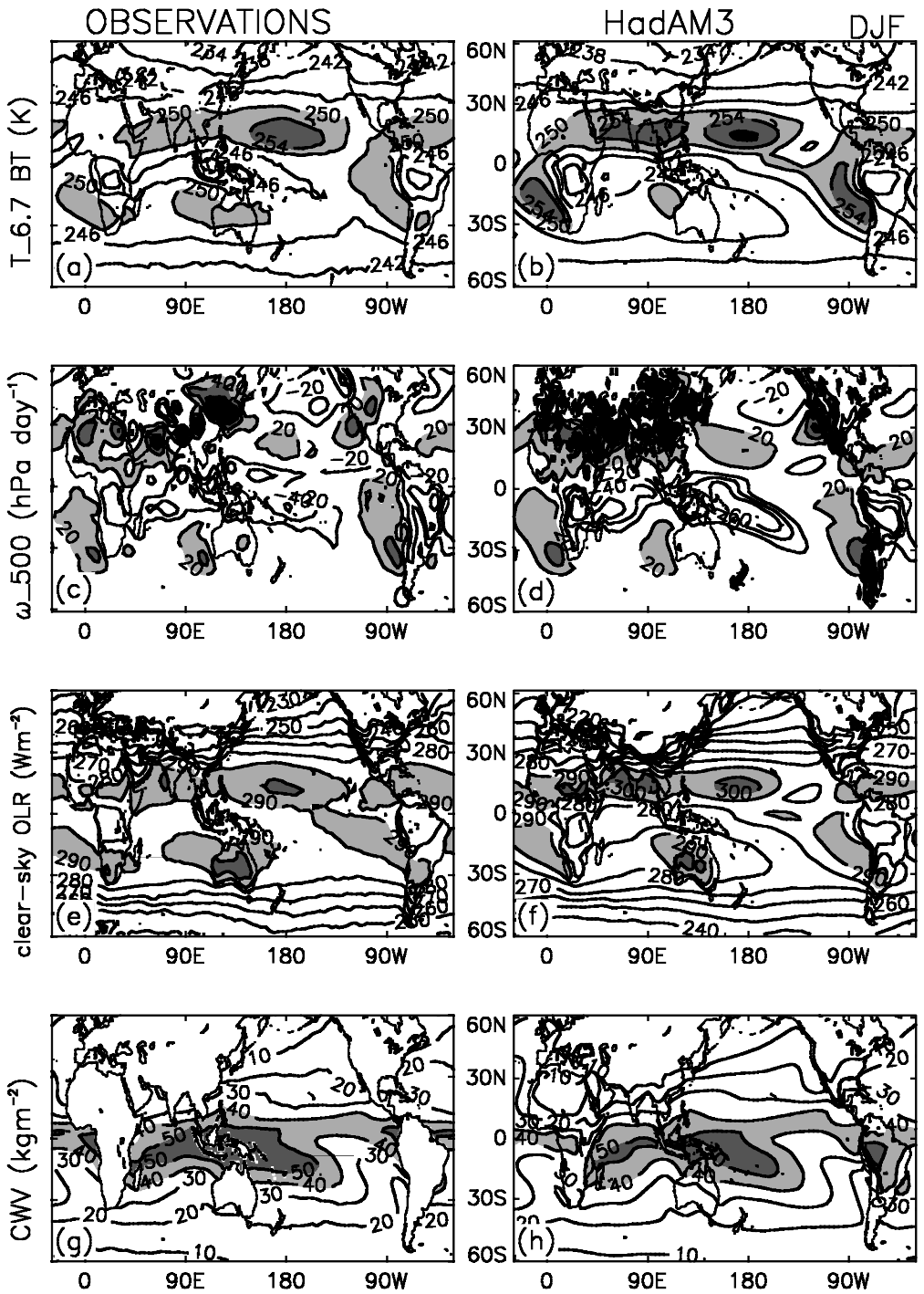


Figure 3. As Fig. 2, but for December–February.

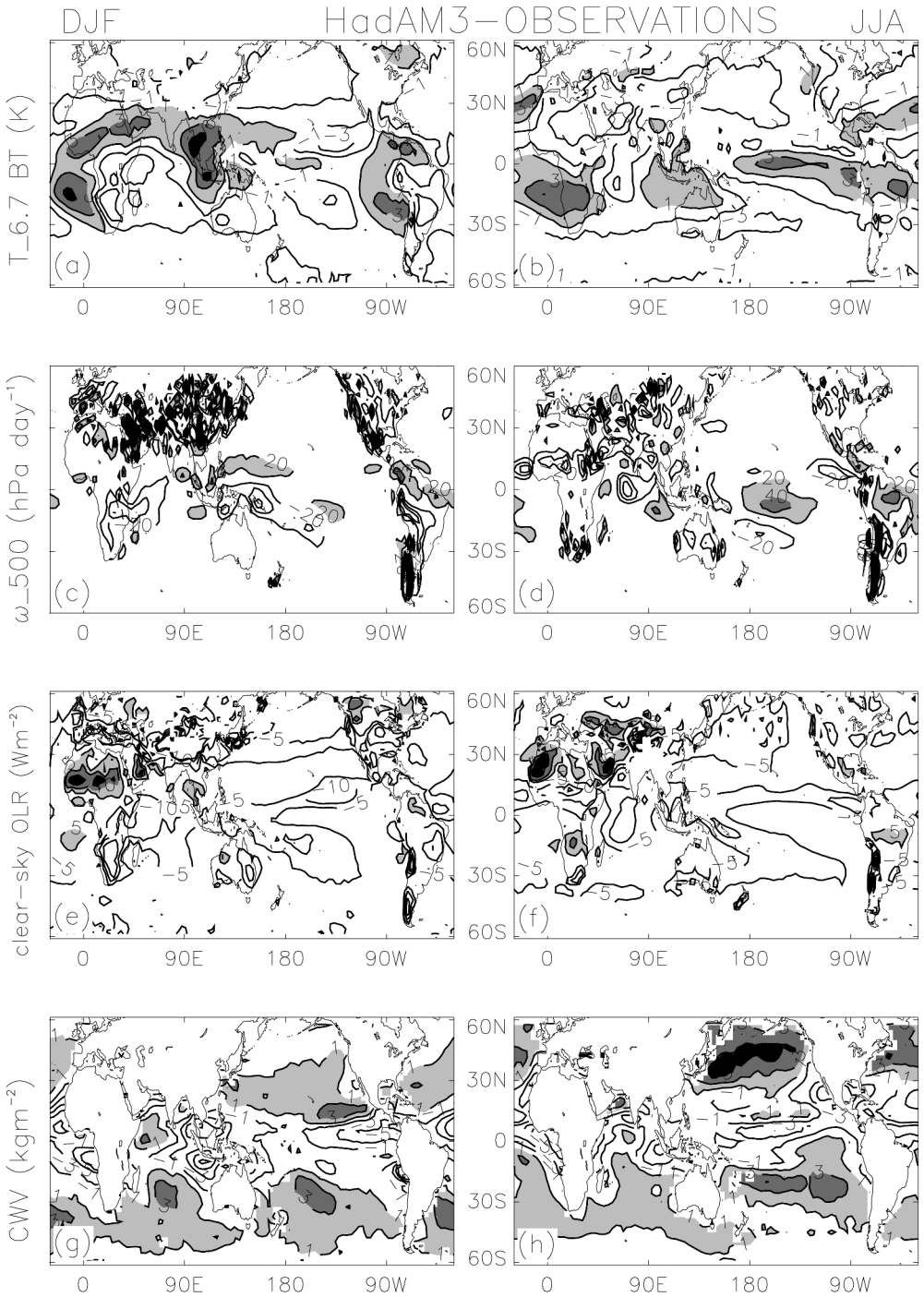


Figure 4. Model-minus-observation difference for fields shown in Figs. 2 and 3: (a)–(b) HadAM3 – HIRS  $6.7 \mu\text{m}$  brightness temperature, (c)–(d) HadAM3 – NCEP 500 hPa vertical velocity, (e)–(f) HadAM3 – ERBS clear-sky outgoing long-wave radiation, and (g)–(h) HadAM3 minus combined SMMR and SSM/I column-integrated water vapour for December–February (left column) and June–August (right column). Positive differences greater than  $T_{6.7} = 1 \text{ K}$ ,  $\omega_{500} = 20 \text{ hPa d}^{-1}$ ,  $\text{OLR} = 5 \text{ W m}^{-2}$  and  $\text{CWV} = 1 \text{ kg m}^{-2}$  are shaded.

control on UTH. Maps of clear-sky OLR (panels (e) and (f)) also show similarities with  $\omega_{500}$  and  $T_{6.7}$ . However, for clear-sky OLR, there is a stronger temperature dependence relating to the emission from low altitudes through the window region of the long-wave spectrum. The CWV is strongly constrained by surface temperature (panels (g) and (h)) with highest moisture content present over the warmest oceans. The model-minus-satellite data CWV differences over the oceans are displayed in Figs. 4(g) and (h). HadAM3 underestimates CWV for the deep Tropics by about  $5 \text{ kg m}^{-2}$  and overestimates CWV over the subtropical open oceans by approximately  $3 \text{ kg m}^{-2}$ . The differences are larger than the expected r.m.s. calibration error of  $1.2 \text{ kg m}^{-2}$  (Wentz 1997). Pope *et al.* (2001) found this bias to reduce on increasing the HadAM3 vertical resolution to 30 levels owing to improved moisture advection.

Because vertical motion exerts a strong control on  $T_{6.7}$ , accurate simulation of brightness temperature will be affected by local model errors in atmospheric circulation. The model-minus-HIRS  $T_{6.7}$  differences (Figs. 4(a) and (b)) do show some correspondence with circulation errors shown in Figs. 4(c) and (d). For example, in DJF stronger descent in HadAM3 compared to NCEP at  $[170^\circ\text{E}, 10^\circ\text{N}]$  corresponds with a positive HadAM3 – HIRS  $T_{6.7}$  bias (Figs. 4(a) and (c)). However, the  $T_{6.7}$  difference fields are characterized primarily by a positive HadAM3 – HIRS bias over regions of mean descent and negative differences at other locations (compare Figs. 2–4). This result also applies to the remaining seasons (not shown). The tendency for dry, subtropical regions to produce higher  $T_{6.7}$  in the simulations compared with the observations is of opposite sign to the mean differences shown in Table 1. It is likely to be an effect of an overvigorous large-scale circulation in HadAM3 (Pope *et al.* 2000) which is also experienced by other models (e.g. Chen *et al.* 1996). However, the sign of the discrepancy is also consistent with cloud contamination of the observations. The effect is particularly evident in the southern hemisphere dry zones which are affected by an overactive South Pacific Convergence Zone and associated Walker circulations (compare the vertical-motion fields in the South Pacific for JJA). Over the South Pacific, the vertical-motion fields simulated by HadAM3 appear rather unrealistic compared to the NCEP data (Figs. 4(c) and (d)). The model also tends to produce stronger ascent in strongly convecting regions compared to NCEP, although this is thought to be an artifact of the NCEP system (Trenberth *et al.* 2000).

The spatial pattern of  $T_{6.7}$  differences is similar to the clear-sky OLR differences if the mean bias calculated in Table 1 is removed from each field (not shown). However, consistent with the mean model clear-sky OLR bias being more negative than the mean  $T_{6.7}$  bias (Table 1), negative differences are geographically more widespread for clear-sky OLR. Locally, the bias roughly doubles when the unmodified clear-sky Type II model diagnostics are analysed (not shown) indicating that the modified sampling removes an important component of the clear-sky sampling inconsistency between HadAM3 and the ERBS satellite. However, it is likely that at least some of this remaining bias stems from subgrid-scale clear-sky sampling biases which cannot be resolved with the data generated in the present study. Alternatively, systematic errors in temperature and moisture profiles in HadAM3 or measurement error may account for some of the differences. The uncertainty for ERBS clear-sky OLR is quoted at  $\pm 5 \text{ W m}^{-2}$  in Barkstrom *et al.* (1989).

#### 4. VARIABILITY

It is clear from Figs. 2–4 that the large-scale circulation determines to a large extent the distributions of UTH and radiative emission to space. In this section we compare the

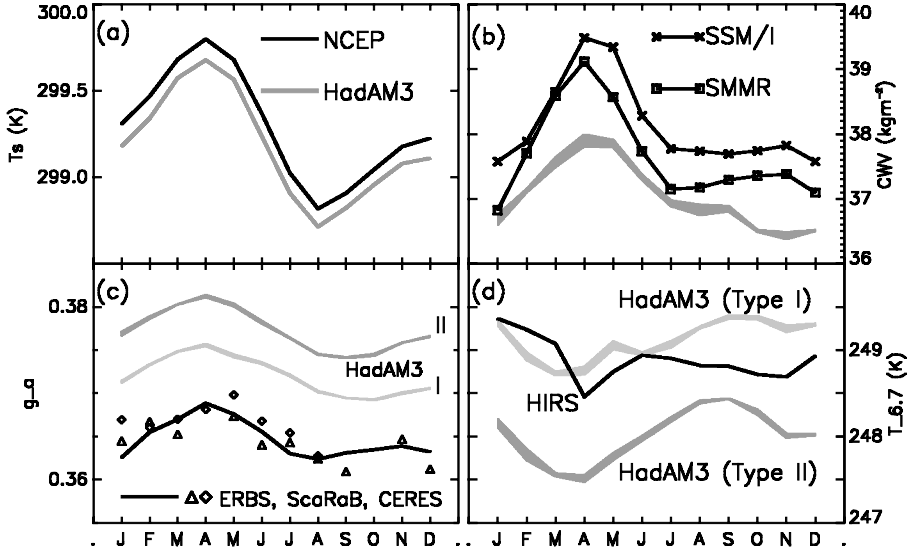


Figure 5. Area-weighted mean monthly climatology over the tropical oceans ( $30^{\circ}\text{S}$ – $30^{\circ}\text{N}$ ) for (a) surface temperature  $T_s$ , (b) column-integrated water vapour, (c) clear-sky normalized greenhouse trapping  $g_a$  and (d) clear-sky  $6.7\ \mu\text{m}$  brightness temperatures  $T_{6.7}$  for HadAM3, NCEP reanalysis and satellite observations. Monthly climatologies are calculated as the mean of the 1979–98 area-weighted averages apart from SMMR (1979–84), SSM/I (1987–98) and ERBS (1985–89). Monthly mean values from ScaRaB and CERES are also displayed. For  $g_a$  and  $T_{6.7}$ , clear-sky Type I and Type II diagnostics are shown for HadAM3—the shaded region denotes the inter-ensemble spread. See text for explanation.

subtle, longer-time-scale signals independent of local vertical motion by considering the variation in moisture averaged over entire circulation systems (see discussion in Lau *et al.* 1996). To ensure meaningful comparisons, we concentrate on the tropical ocean. This allows a large enough coverage to remove most of the effect of changes in mean vertical motion on the moisture and radiation fields. Also the satellite data coverage is most reliable and extensive over the tropical oceans.

#### (a) Seasonal variability

Figure 5 shows the seasonal variation of surface temperature, CWV, normalized clear-sky greenhouse trapping  $g_a$  (Raval and Ramanathan 1989) and  $T_{6.7}$  over the tropical oceans ( $30^{\circ}\text{S}$ – $30^{\circ}\text{N}$ ) for the observationally based data and HadAM3 (the grey region encompasses the three ensemble members). We calculate  $g_a$  as the difference between the area-mean clear-sky OLR,  $\overline{\text{OLR}_c}$ , and the surface emission, normalized by the area-mean surface emission:

$$g_a = (\overline{\sigma T_s^4} - \overline{\text{OLR}_c}) / (\overline{\sigma T_s^4}), \quad (2)$$

where  $\sigma$  is the Stefan Boltzmann constant and  $T_s$  is the surface temperature. We use  $g_a$  because this provides a good measure of the water-vapour greenhouse effect while the clear-sky OLR signal is affected both by humidity and surface temperature (e.g. Allan *et al.* 1999).

The maximum in column water vapour occurs in April, coinciding with the highest tropical ocean temperatures. The observed CWV is larger than the simulated values by about 5%. Mean SSM/I values are nearly  $0.5\ \text{kg m}^{-2}$  higher than those of SMMR. The difference is consistent with  $0.11\ \text{K}$  higher SSTs during the later SSM/I period

(1988–98) compared with the SMMR period (1979–84). When the simulated climatologies are sampled separately for each period, the post 1987 period is  $0.4 \text{ kg m}^{-2}$  moister than the pre-1985 period. The maximum CWV also coincides with the greatest atmospheric greenhouse trapping in the model and observations, consistent with the strongest water-vapour greenhouse effect and the minimum in  $T_{6,7}$  in April.

The bias between observations and simulations of clear-sky  $g_a$  and  $T_{6,7}$  is noticeably smaller for the modified Type I diagnostics compared to the standard Type II clear-sky diagnostics. However, a sizeable  $g_a$  bias remains for the clear-sky Type I diagnostics. It is not as yet clear whether this bias relates to model errors, satellite uncertainty or a residual subgrid-scale clear-sky sampling inconsistency. The scatter of ScaRaB and CERES monthly mean  $g_a$  about the ERBS climatology illustrates the differences due to the combination of satellite calibration errors and interannual variability. Because ScaRaB and CERES used a similar clear-sky detection method to ERBS, differences relating to clear-sky sampling inconsistencies are likely to be small and relate primarily to satellite pixel size (Wielicki *et al.* 1996). The simulations display a similar seasonal variation of CWV and  $g_a$  to the satellite data over the tropical oceans. However, the simulated changes in  $T_{6,7}$  do not correspond well with the observed changes. Nevertheless, seasonal changes in  $T_{6,7}$  in both model and observations are small, varying by less than 0.5% of the mean. This indicates small tropical mean UTH variation in the observations and model.

### (b) *Interannual variability*

(i) *Tropical oceans.* To evaluate the longer-time-scale variability of water vapour in HadAM3, interannual anomalies were calculated by removing the seasonal cycles presented in Fig. 5. The anomalies of surface temperature, column water vapour, normalized greenhouse trapping and  $T_{6,7}$  are presented in Fig. 6. The time series are smoothed using a five-month moving window to emphasize the interannual fluctuations. For the column water-vapour data, anomalies were calculated with respect to the combined SSM/I and SMMR seasonal climatology, while ScaRaB and CERES  $g_a$  anomalies were calculated with respect to the ERBS 1985–89 mean seasonal cycle. All other interannual anomalies were calculated relative to the full 1979–98 climatologies. Constructing model climatologies from the same years as the corresponding observations does not alter the results significantly. An important result relates to the similarity between Type I and Type II clear-sky model diagnostics for  $g_a$  (Fig. 6(c)) and  $T_{6,7}$  (Fig. 6(d)). While clear-sky sampling details strongly affect the local differences in clear-sky OLR and  $T_{6,7}$ , these differences and the more subtle differences present in the seasonal variability (Fig. 5) are removed when considering interannual anomalies.

Figure 6(a) shows the variability of tropical ocean temperatures to be dominated by the El Niño warm events, which are particularly evident in the DJF season of 1979–80, 1982–83, 1986–87 and 1997–98. Corresponding peaks in CWV are present at these times in the observations and the model simulations. The anomalously high CWV amounts are characterized by an intense moist zone across the equatorial eastern Pacific and also higher CWV over the Indian and Atlantic tropical oceans (not shown). The simulated decadal fluctuations in CWV show excellent agreement with the combined record of microwave satellite data (agreement for  $50^\circ\text{S}$ – $50^\circ\text{N}$  oceans is also excellent). The model gives a similar sensitivity of CWV to  $T_s$  as the satellite observations (about  $3.5 \text{ kg m}^{-2}\text{K}^{-1}$ ) with a correlation coefficient,  $r = 0.86$  (see also Wentz and Schabel 2000).

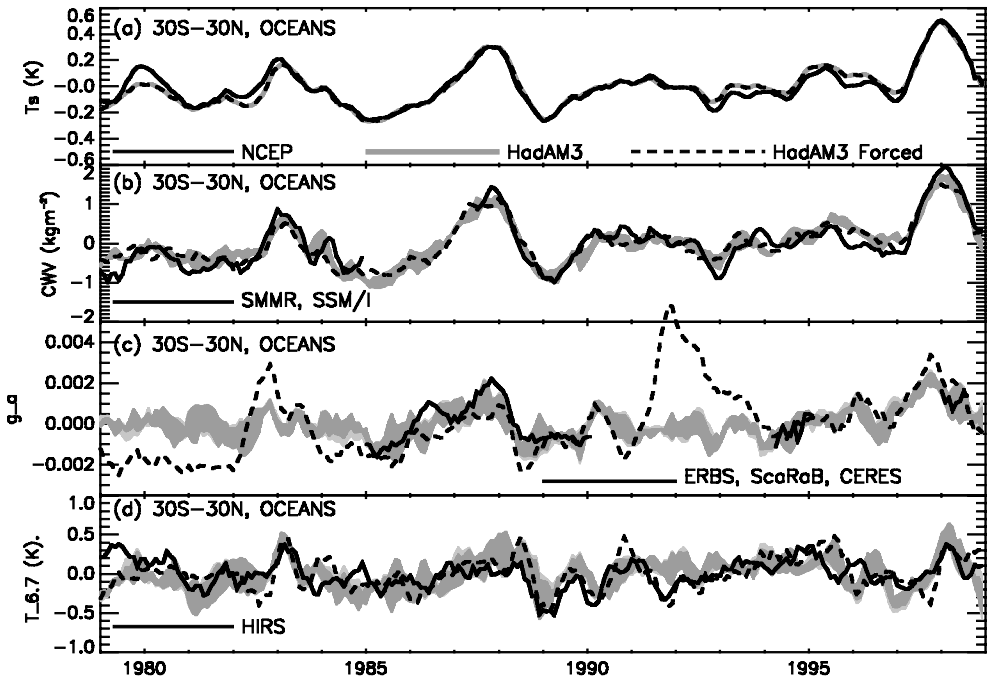


Figure 6. Interannual anomalies of (a) surface temperature, (b) column water vapour, (c) normalized greenhouse trapping and (d)  $6.7 \mu\text{m}$  brightness temperature for area-weighted means over the tropical oceans. Anomalies are formed by removing the monthly climatology displayed in Fig. 5. The shaded region denotes inter-ensemble spread for HadAM3 SST-only forcing. Dark and light shading denote Type I and Type II diagnostics, respectively (see text). The dashed line denotes the ‘all-forcings’ HadAM3 experiment.

A peak in observed  $g_a$  over the tropical oceans during the 1987 El Niño warm event is captured by HadAM3. However, an additional peak in observed greenhouse trapping during 1986 does not appear in the model simulations. Comparing these observations over similar space and time-scales, Soden (1997) showed the Geophysical Fluid Dynamics Laboratory model captured both peaks in  $g_a$ , explaining the secondary maxima during 1986 in terms of a dynamical response to the changes in SST distribution. There is a positive correlation between observed greenhouse trapping and  $T_s$  (significant at the 95% level allowing for autocorrelation) with  $g_a$  increasing at the rate of  $4 \times 10^{-3} \text{ K}^{-1}$ . This positive correlation for HadAM3 is also significant but slightly weaker. The observed  $g_a$  anomalies are in excellent agreement with the model values. This agreement is particularly interesting in light of the observed large decadal changes in tropical mean all-sky OLR which are not simulated by climate models (Wielicki *et al.* 2002). The stability of the observed clear-sky OLR signal indicates that calibration errors are unlikely to explain such a discrepancy, suggesting that models, even those to which realistic forcings are applied, cannot simulate the decadal changes in cloudiness (e.g. Allan and Slingo 2002). Alternatively, calibration differences between the satellite instruments are offset by sampling differences in the clear-sky OLR record between ERBS, ScaRaB and CERES.

Considering the all-forcings HadAM3 experiment (dashed lines in Fig. 6) we find that the simulated  $g_a$  variability is highly sensitive to the input of volcanic aerosol following the El Chichon eruption in 1982 and the Pinatubo eruption in 1991. A positive trend in  $g_a$  over the 1979–98 period is related to the increased greenhouse trapping of

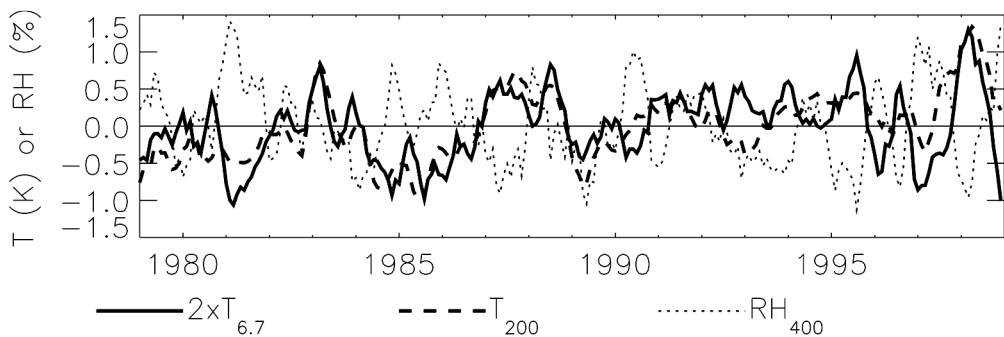


Figure 7. Interannual anomalies of 200 hPa atmospheric temperature  $T_{200}$ , 400 hPa relative humidity  $RH_{400}$  and  $T_{6,7}$  for  $30^{\circ}\text{S}$ – $30^{\circ}\text{N}$  area-weighted means over the oceans.

the atmosphere as greenhouse-gas concentrations rise. The simulated  $T_{6,7}$  and CWV variability are relatively insensitive to such additional forcings. However, the prescription of volcanic aerosol in the all-forcings HadAM3 scenario appears to improve the simulation of the drop in  $T_{6,7}$  following the Pinatubo eruption in 1991 (see also Soden *et al.* 2002). Neither the observed nor the simulated  $T_{6,7}$  variability show significant correlation to changes in  $T_s$ . The magnitude of the simulated interannual variability of  $T_{6,7}$  is consistent with the HIRS observations (Fig. 6(d)). Further, many aspects of the observed variability are well simulated by HadAM3, for example the 1983 and 1998 El Niño events and the 1989 cold event.

(ii) *Dependence of  $T_{6,7}$  on temperature and humidity variation.* While  $T_{6,7}$  is strongly sensitive to relative humidity in the upper troposphere, Eq. (1) also contains terms relating to the temperature profile. While previous studies (e.g. Soden and Bretherton 1993; Jackson and Bates 2001) have determined the relationship between UTH and  $T_{6,7}$  spatially, it does not necessarily follow that this spatial correlation is relevant for the tropical-mean changes. While we cannot directly validate that the observed 1979–98 variations in tropical-mean  $T_{6,7}$  are representative of the mean UTH changes, we can check this for the model data.

Figure 7 shows time series of  $T_{6,7}$ , 200 hPa temperature  $T_{200}$  and 400 hPa relative humidity  $RH_{400}$  for HadAM3 over the tropical oceans. Anomalies of  $RH_{400}$  are generally negatively correlated with those of  $T_{6,7}$ , as expected. However, changes in  $T_{200}$  are positively correlated with those in  $T_{6,7}$ . Applying a multiple linear regression on the interannual anomalies shown in Fig. 6 gives the following relationship and standard error estimates:

$$T_{6,7} = (0.29 \pm 0.14)T_{200} - (0.25 \pm 0.12)RH_{400}. \quad (3)$$

Both  $T_{200}$  and  $RH_{400}$  explain about one third of the total variability in  $T_{6,7}$ ;  $T_{200}$  is not significantly correlated with  $RH_{400}$ . This suggests that, while  $T_{6,7}$  is a good indicator of changes in UTH, over the tropical-mean interannual time-scale, changes in upper-tropospheric temperature are equally important. If HadAM3 accurately simulates the changes in tropical tropospheric temperature, then the agreement between observed and simulated  $T_{6,7}$  helps to validate the model changes in tropical-mean UTH. Soden (2000a) showed that a multi-model ensemble of atmospheric general-circulation models forced by SST could generally capture the tropical-mean changes in  $T_{200}$  derived from radiosonde measurements. Indeed, comparison of Fig. 7 with Fig. 4 of Soden

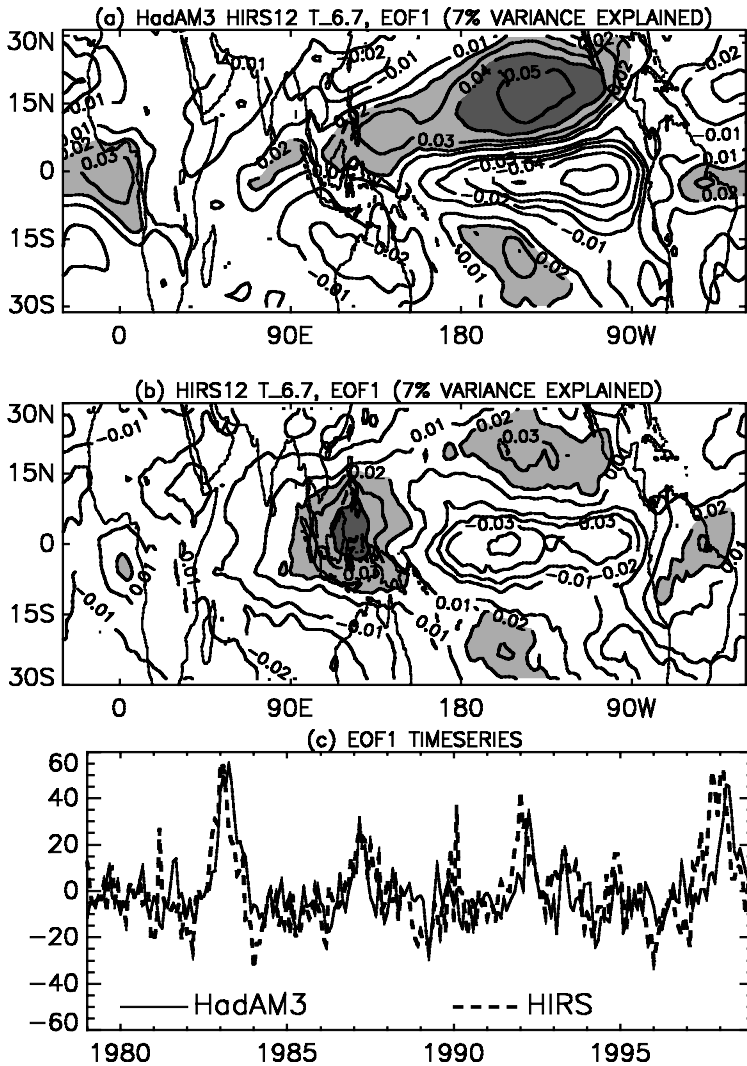


Figure 8. First EOF pattern applied to  $6.7 \mu\text{m}$  brightness temperature for (a) HadAM3 and (b) HIRS observations; (c) the corresponding time series.

(2000a) shows the variation of  $T_{200}$  in HadAM3 to be consistent with the observed variability. However, model underestimation of  $T_{200}$  anomalies prior to 1981 also coincides with an underestimation in  $T_{6.7}$  as shown in Fig. 6. Thus, care must be taken when interpreting changes in interannual changes in tropical-mean UTH from  $6.7 \mu\text{m}$  emission.

(iii) *EOF analysis.* The previous sections have shown the simulations of  $T_{6.7}$  to be in reasonable agreement with the observations when considering spatial climatologies and considering the interannual variations. We now characterize the spatio-temporal variability by computing the leading empirical orthogonal functions (EOFs) of  $T_{6.7}$  for the observations and simulations. For consistency with Fig. 2 of Bates *et al.* (2001), we consider deseasonalized tropical data ( $30^{\circ}\text{S}$ – $30^{\circ}\text{N}$ ).

Figure 8 shows the leading EOFs for  $T_{6.7}$ , simulated by HadAM3 and measured by HIRS, and the EOF time series. There is excellent agreement between the model and the observations, with the El Niño warm events of 1982–83, 1987–88 and 1997–98 producing higher than average  $T_{6.7}$  over the tropical west Pacific and over the central subtropical Pacific. This relates to a change in the large-scale circulation, such that convection usually over the tropical west Pacific moves over the central Pacific (lower than average  $T_{6.7}$ ) which in turn induces extra descent over adjacent regions. This situation is also apparent in both model and observations during 1992, although this is not visible on the interannual anomaly time series in Fig. 6, possibly due to the effects of Mount Pinatubo on SSTs. The model appears to overestimate the magnitude of the  $T_{6.7}$  signal, particularly over the subtropical Pacific between Hawaii and Baja California. Conversely, Salathé *et al.* (1995) found their model simulations to underestimate the  $T_{6.7}$  anomalies in this area during the 1982–83 El Niño compared to the observations. The differences with the observations may reflect inadequacy of the models in capturing the transient wave activity and its interaction with ENSO in these regions (e.g. Bates *et al.* 2001). However, the excellent agreement in the spatial signature of interannual variability shows that the gross El Niño-related SST anomalies prescribed in the simulations are sufficient to force a realistic spatial shift in the large-scale circulation and corresponding UTH distributions.

## 5. CONCLUSIONS

The distribution and variability of moisture, simulated in an atmosphere-only climate model (HadAM3), are evaluated using satellite retrievals of column-integrated water vapour CWV, clear-sky OLR and  $6.7 \mu\text{m}$  brightness temperatures  $T_{6.7}$ . In particular we concentrate on the comparison with HIRS  $T_{6.7}$  observations which provide information on upper-tropospheric relative humidity over the period 1979–98. The  $6.7 \mu\text{m}$  radiances required for such a comparison are computed explicitly at each radiation time step (3 h) of the model integration over the entire model grid. To enhance the comparisons we additionally produce modified clear-sky OLR and  $T_{6.7}$  diagnostics which have been adjusted to reduce clear-sky sampling inconsistencies between the satellite measurements and HadAM3.

The distribution and variability of the satellite data are reasonably well simulated by HadAM3. Also well captured are the spatial signature of the interannual variations of  $T_{6.7}$ , primarily relating to changes in large-scale atmospheric circulation over the El Niño cycle. The r.m.s. bias in the  $60^\circ\text{S}$ – $60^\circ\text{N}$  seasonal climatology of  $T_{6.7}$  is less than 2 K or about 0.7% of the area-weighted mean, consistent with a similar analysis of the NCAR model by Iacono *et al.* (2003). The model overestimates  $6.7 \mu\text{m}$  emission in the dry subtropical regions, particularly in the southern hemisphere. This is symptomatic of an overly vigorous circulation and is compounded by a rather unrealistic simulated vertical-motion pattern in the South Pacific compared to the NCEP reanalysis. However, it is also possible that cloud contamination of the HIRS radiances may also contribute to this discrepancy. The model also appears to underestimate CWV in the deep Tropics and overestimate CWV over midlatitude oceans compared to satellite microwave measurements, consistent with excessive moisture export from the Tropics.

The modified clear-sky diagnostics significantly reduce the negative model-minus-observations difference for clear-sky OLR and  $T_{6.7}$ . However, a significant bias remains for clear-sky OLR which is either related to unrealistic atmospheric properties in HadAM3, observational uncertainty or additional sampling inconsistencies. However,

without knowledge of subgrid-scale moisture differences between overcast and clear regions, the satellite sampling bias cannot be quantified more accurately. Nevertheless, the effect of the clear-sky sampling bias on simulated interannual variability is negligible.

Interannual variations in CWV from 1979–98 are well simulated by HadAM3 in agreement with previous studies over a more limited period (e.g. Soden 2000a). Fluctuations of tropical ocean mean  $T_{6,7}$  are small (about  $\pm 0.5$  K) and of a consistent magnitude on an interannual time-scale between the observations and simulations. Changes in upper-tropospheric temperature, in addition to relative humidity, also influence the interannual variation of mean  $T_{6,7}$  over the tropical oceans. However, the consistent variability of  $T_{6,7}$  and clear-sky OLR between model and observations suggests that the small decadal changes in relative humidity simulated by HadAM3 are realistic, as argued in recent studies of water-vapour feedback (e.g. Ingram 2002; Soden *et al.* 2002). The issue of observed and simulated variations in tropical cloudiness remains unresolved at present (e.g. Wielicki *et al.* 2002). Further careful analysis is required to confirm the robust nature of the interannual variability of relative humidity and cloudiness, particularly with respect to the correction of satellite orbit and calibration drifts.

#### ACKNOWLEDGEMENTS

This work was funded by the Department for Environment, Food and Rural Affairs under contract PECD 7/12/37. The ERBS data were retrieved from the National Aeronautics and Space Administration (NASA) Langley DAAC, the SMMR data from the NASA Jet Propulsion Laboratory DAAC, the NCEP reanalysis data from the National Oceanic Atmospheric Administration/Cooperative Institute for Research in the Environmental Sciences Climate Diagnostics Center, the SSM/I data from <http://www.ssmi.com/> and the ScaRaB data was provided by the Centre National d'Etudes Spatiales, Toulouse. The HIRS brightness temperatures were provided by Helen Brindley and Darren Jackson. Thanks to John Edwards for help with the radiance code and to William Ingram for suggesting the clear-sky fraction weighting diagnostic. Two anonymous reviewers are thanked for their useful suggestions.

#### REFERENCES

- |  |      |  |
|--|------|--|
| Allan, R. P. and Ringer, M. A.   | 2003 | Inconsistencies between satellite estimates of longwave cloud forcing and dynamical fields from reanalyses. <i>Geophys. Res. Lett.</i> , <b>30</b> , 1491, doi:10.1029/2003GL017019  |
| Allan, R. P. and Slingo, A.  | 2002 | Can current climate forcings explain the spatial and temporal signatures of decadal OLR variations? <i>Geophys. Res. Lett.</i> , <b>29</b> , 1141, doi:10.1029/2001GL014620  |
| Allan, R. P., Shine, K. P., Slingo, A. and Pamment, J. A.  | 1999 | The dependence of clear-sky outgoing long-wave radiation on surface temperature and relative humidity. <i>Q. J. R. Meteorol. Soc.</i> , <b>125</b> , 2103–2126   |
| Allan, R. P., Ramaswamy, V. and Slingo, A.   | 2002 | Diagnostic analysis of atmospheric moisture and clear-sky radiative feedback in the Hadley Centre and Geophysical Fluid Dynamics Laboratory (GFDL) climate models. <i>J. Geophys. Res.</i> , <b>107</b> , 4329, doi:10.1029/2001JD001131 |
| Barkstrom, B., Harrison, E., Smith, G., Green, R., Kibler J., Cess, R. and the ERBE Science Team | 1989 | Earth Radiation Budget Experiment (ERBE) archival and April 1985 results. <i>Bull. Am. Meteorol. Soc.</i> , <b>70</b> , 1254–1262  |
| Bates, J. J. and Jackson, D. L.  | 1997 | A comparison of water vapor observations with AMIP I simulations. <i>J. Geophys. Res.</i> , <b>102</b> , 21837–21852   |
|  | 2001 | Trends in upper tropospheric humidity. <i>Geophys. Res. Lett.</i> , <b>28</b> , 1695–1698  |

- Bates, J. J., Jackson, D. L., Breon, F.-M. and Bergen, Z. D. 2001 Variability of tropical upper tropospheric humidity 1979–1998. *J. Geophys. Res.*, **106**, 32271–32281
- Bauer, N., Del Genio, A. D. and Lanzante, J. R. 2002 Observed and simulated temperature–humidity relationships: Sensitivity to sampling and analysis. *J. Climate*, **15**, 203–215
- Cess, R. D. and Potter, G. L. 1987 Exploratory studies of cloud radiative forcing with a general circulation model. *Tellus*, **39**, 460–473
- Chen, C.-T., Roeckner, E. and Soden, B. J. 1996 A comparison of satellite observations and model simulations of column integrated moisture and upper tropospheric humidity. *J. Climate*, **9**, 1561–1585
- Edwards, J. M. and Slingo, A. 1996 Studies with a flexible new radiation code. I: Choosing a configuration for a large-scale model. *Q. J. R. Meteorol. Soc.*, **122**, 689–719
- Elliot, W. P. 1995 On detecting long-term changes in atmospheric moisture. *Climate Change*, **31**, 349–367
- Engelen, R. J., Fowler, L. D., Gleckler, P. J. and Wehner, M. F. 2000 Sampling strategies for the comparison of climate model calculated and satellite observed brightness temperatures. *J. Geophys. Res.*, **105**, 9393–9406
- Held, I. M. and Soden, B. J. 2000 Water vapor feedback and global warming. *Ann. Rev. Energy Environ.*, **25**, 441–475
- Iacono, M. J., Delamere, J. S., Mlawer, E. J. and Clough, S. A. 2003 Evaluation of upper tropospheric water vapor in the NCAR Community Climate Model (CCM3) using modeled and observed HIRS radiances. *J. Geophys. Res.*, **108**, 4037, doi:10.1029/2002JD002539
- Ingram, W. J. 2002 On the robustness of the water vapor feedback: GCM vertical resolution and formulation. *J. Climate*, **15**, 917–921
- IPCC 2001 *Climate change 2001: The scientific basis*. Eds. J. T. Houghton, Y. Ding, D. J. Griggs, M. Noguer, P. J. van der Linden, X. Dai, K. Maskell and C. A. Johnson. Cambridge University Press
- Jackson, D. L. and Bates, J. J. 2001 Upper tropospheric humidity algorithm assessment. *J. Geophys. Res.*, **106**, 32259–32270
- Kalnay, E. M., Kanamitsu, M., Kistler, R., Collins, W., Deaven, D., Gandin, L., Iredell, M., Saha, S., White, G., Woollen, J., Zhu, Y., Chelliah, M., Ebisuzaki, W., Higgins, W., Janowiak, J., Mo, K. C., Ropelewski, C., Wang, J., Leetmaa, A., Reynolds, R., Jenne, R. and Joseph, D. 1996 The NCEP/NCAR 40-year reanalysis project. *Bull. Am. Meteorol. Soc.*, **77**, 437–471
- Kandel, R. and the International ScaRaB Scientific Working Group (ISSWG) 1998 The ScaRaB radiation budget dataset. *Bull. Am. Meteorol. Soc.*, **79**, 765–783
- Lanzante, J. R. and Gahrs, G. E. 2000 The ‘clear-sky bias’ of TOVS upper-tropospheric humidity. *J. Climate*, **13**, 4034–4041
- Lau, K.-M., Ho, C.-H. and Chou, M.-D. 1996 Water vapor and cloud feedback over the tropical oceans: Can we use ENSO as a surrogate for climate change? *Geophys. Res. Lett.*, **23**, 2971–2974
- Li, D. and Shine, K. P. 1995 ‘A 4-dimensional ozone climatology for UGAMP models’. UGAMP Internal Report No. 35
- Pope, V. D., Gallani, M. L., Rowntree, P. R. and Stratton, R. A. 2000 The impact of new physical parametrizations in the Hadley Centre Climate Model—HadAM3. *Clim. Dyn.*, **16**, 123–146
- Pope, V. D., Pamment, J. A., Jackson, D. R. and Slingo, A. 2001 The representation of water vapor and its dependence on vertical resolution in the Hadley Centre Climate Model. *J. Climate*, **14**, 3065–3085
- Raval, A. and Ramanathan, V. 1989 Observational determination of the greenhouse effect. *Nature*, **342**, 758–761
- Rayner, N. A., Parker, D. E., Horton, E. B., Folland, C. K., Alexander, L. V., Rowell, D. P., Kent, E. C. and Kaplan, A. 2003 Global analysis of SST, sea ice and night marine air temperature since the late nineteenth century. *J. Geophys. Res.*, **108**, 4407 doi:10.1029/2002JD002670
- Ringer, M. A., Edwards, J. M. and Slingo, A. 2002 Simulation of satellite channel radiances in the Met Office Unified Model. *Q. J. R. Meteorol. Soc.*, **129**, 1169–1190

- Salathé, E. P., Chesters, D. and Sud, Y. C. 1995 Evaluation of the upper-tropospheric moisture climatology in a general circulation model using TOVS radiance observations. *J. Climate*, **8**, 2404–2414
- Shine, K. P. and Sinha, A. 1991 Sensitivity of the earth's climate to height-dependent changes in water-vapour mass mixing ratio. *Nature*, **354**, 382–384
- Soden, B. J. 1997 Variations in the tropical greenhouse effect during El Niño. *J. Climate*, **10**, 1050–1055
- 2000a The sensitivity of the tropical hydrological cycle to ENSO. *J. Climate*, **13**, 538–549
- 2000b The diurnal cycle of convection, clouds, and water vapor in the tropical upper troposphere. *Geophys. Res. Lett.*, **27**, 2173–2176
- Soden, B. J. and Bretherton, F. P. 1993 Upper tropospheric relative humidity from the GOES 6.7  $\mu\text{m}$  channel: Method and climatology for July 1987. *J. Geophys. Res.*, **98**, 16669–16688
- Soden, B. J. and Fu, R. 1995 A satellite analysis of deep convection, upper tropospheric humidity and the greenhouse effect. *J. Climate*, **8**, 2333–2351
- Soden, B. J., Wetherald R. T., Stenchikov, G. L. and Robock, A. 2002 Global cooling after the eruption of Mount Pinatubo: A test of climate feedback by water vapor. *Science*, **296**, 727–730
- Spencer, R. W. and Braswell, W. D. 1997 How dry is the tropical free troposphere? Implications for global warming theory. *Bull. Am. Meteorol. Soc.*, **78**, 1097–1106
- Sun, D.-Z. and Held, I. M. 1996 A comparison of modeled and observed relationships between inter-annual variations of water vapor and temperature. *J. Climate*, **9**, 665–675
- Trenberth, K. E., Stepaniak, D. P., Hurrell, J. W. and Fiorino, M. 2001 Quality of re-analyses in the Tropics. *J. Climate*, **14**, 1499–1510
- Udelhofen, P. M. and Hartmann, D. L. 1995 Influence of tropical cloud systems on the relative humidity in the upper troposphere. *J. Geophys. Res.*, **100**, 7423–7440
- Wentz, F. J. 1997 A well-calibrated ocean algorithm for SSM/I. *J. Geophys. Res.*, **102**, 8703–8718
- Wentz, F. J. and Francis, E. A. 1992 'Nimbus-7 SMMR ocean products 1979–1984'. Remote Sensing Systems Technical Report No. 033192. Available from Remote Sensing Systems, 1011 College Ave., Santa Rosa, CA 95404, USA
- Wentz, F. J. and Schabel, M. 2000 Precise climate monitoring using complementary satellite data sets. *Nature*, **403**, 414–416
- Wielicki, B. A., Barkstrom, B. R., Harrison, E. F., Lee, R. B., Smith, G. L. and Cooper, J. E. 1996 Clouds and the Earth's Radiant Energy System (CERES): An Earth observing system experiment. *Bull. Am. Meteorol. Soc.*, **77**, 853–868
- Wielicki, B. A., Wong, T., Allan, R. P., Slingo, A., Kiehl, J. T., Soden, B. J., Gordon, C. T., Miller, A. J., Yang, S.-K., Randall, D. A., Robertson, F., Susskind, J. and Jacobowitz, H. 2002 Evidence for large decadal variability in the tropical mean radiative energy budget. *Science*, **295**, 841–844
- Yang, G. Y. and Slingo, J. M. 2001 The diurnal cycle in the Tropics. *Mon. Weather Rev.*, **129**, 784–801